ACS Macro Letters

Cite This: ACS Macro Lett. 2018, 7, 447−452

Letter

pubs.acs.org/macroletters

Trefoil Knot Hydrodynamic Delocalization on Sheared Ring Polymers

Maximilian Liebetreu,*[,†] Marisol Ripoll,[‡] and Christos N. Likos[†]

[†]Faculty of Physics, University of Vienna, Boltzmanngasse 5, 1090 Vienna, Austria

[‡]Forschungszentrum Jülich, Institute of Complex Systems, Theoretical Soft Matter and Biophysics, 52425 Jülich, Germany

Supporting Information

ABSTRACT: The behavior of unknotted and trefoil-knotted ring polymers under shear flow is here examined by means of mesoscopic simulations. In contrast to most polymers, ring polymers in a hydrodynamic solvent at high shear rates do not get shortened in the vorticity direction. This is a consequence of the backflow produced by the interaction of the sheared solvent with the end-free polymer topology. The extended structures of the ring in the vorticity-flow plane, when they are aligned in a constant velocity plane, favor ring contour fluctuations. This variety of conformations largely suppresses the tank-treading type of rotation with extended conformations in favor of the tumbling type of rotations, where stretched and collapsed conformations alternate. The extension of trefoil knots is also enhanced, so that the knots become delocalized. We anticipate that these effects, which disappear in the absence of hydrodynamic interactions, will have a crucial impact on the rheological properties of concentrated ring solutions, and will also influence the behavior of more complicated systems such as mixtures of polymers with different topologies.

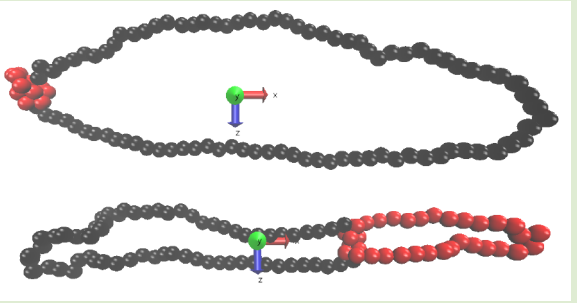

Investigations on the out-of-equilibrium dynamics of dilute and concentrated solutions of soft and deformable colloids have experienced a dramatic increase in the past decade, both theoretically and experimentally.[1,2] The notion of "soft colloids" encompasses a large variety of polymer-based nanoparticles, such as linear chains, star polymers and brushes, dendrimers, and microgels, but it also extends to larger objects such as vesicles, emulsions, and red blood cells. The main pertinent issues of interest include, the connection between molecular architecture, deformation, and dynamics under shear, and then the consequences of the same on stress distribution, viscosity, rheology, and thixotropic behavior of sheared concentrated solutions. Parallel to the investigations on polymer architecture on structure and dynamics, there has been a dramatic increase in the efforts to understand the influence of polymer topology on the same.[3−6] Of particular interest are topologically quenched knots (self-links) that exist on a closed (ring-shaped) polymer, and the properties they impact on the conformations and dynamics of the macromolecule. The probability of obtaining unknotted configurations is decreasing exponentially with the polymer contour length.[7] Knots occur naturally on long DNA strands[8−10] and on proteins,[11−13] whereas optical tweezers can also be used to tie specific knots on DNA-molecules in a controlled fashion.[14,15] Synthetic chemists have developed a series of strategies to create molecular knots of well-defined topology by using molecules specifically designed for this purpose.[16]

A great deal of attention has been paid to the equilibrium properties of polymer knots and their relaxation dynamics in the bulk,[17−25] in confinement[26−35] and under tension.[36−41] Regarding the nonequilibrium dynamics of the same, a considerable amount of work has focused on knot translocation[42−49] and on the behavior of knots under elongational flow.[50,51] Very little is known about a different but very common out-of-equilibrium situation, namely, the behavior of knots under steady shear. Here, numerical work has been devoted exclusively to non-Brownian polymers and Stokes flow;[52,53] investigations on the flow behavior of ring polymers with fully developed hydrodynamics and in the presence of thermal noise have been limited, at this point, to unknotted rings.[54−59] The purpose of this work is to shed light on the question of the interplay between topology and hydrodynamics for knotted or unknotted rings in a solvent undergoing planar Couette flow. A nontrivial coupling between hydrodynamics and topology manifests itself, both for unknotted (0_1)- and trefoil-knotted (3_1)-rings, which essentially maintains the equilibrium size of the ring in the vorticity direction, in contrast to polymers with ends. These noncompressed configurations lead to knot delocalization at sufficiently high Weissenberg numbers. This phenomenon is accompanied by a suppression of tank-treading motions, which favor localized knots, and a predominance of tumbling dynamics during which the knot is distributed across the molecule. In the absence of hydrodynamics, or in the absence of the closure of the molecule, the polymer rings decrease in size along the vorticity direction and the associated phenomenology for the knots disappears, underlying the crucial role played by the

Received: January 22, 2018
Accepted: March 20, 2018

DOI: 10.1021/acsmacrolett.8b00059
ACS Macro Lett. 2018, 7, 447−452

simultaneous presence of both for ring polymers under shear in a Newtonian solvent.

We performed Multi-Particle Collision Dynamics (MPCD) simulations[60−64] to ensure that hydrodynamic interactions (+HI) between the monomers are included. Lees-Edwards boundary conditions[65] and a Maxwellian cell-level thermostat[66] were used to maintain the linear velocity profile of planar Couette flow with shear rate $\dot{\gamma}$ at fixed temperature. The solvent velocity has the form $\mathbf{v}_s = \dot{\gamma}\, y\, \hat{\mathbf{x}}$, defining thereby $(\hat{\mathbf{x}},\hat{\mathbf{y}},\hat{\mathbf{z}})$ as the flow, gradient, and vorticity directions, respectively. Molecular Dynamics (MD) was used to simulate fully flexible polymers of $N = 100$ monomer beads, employing a bead−spring model[67,68] and making use of the Velocity-Verlet algorithm[69] to solve the equations of motion, coupled to the solvent using the collision step of MPCD.[70] To precisely distinguish the influence of hydrodynamics, we performed additional simulations with a solvent modeled by the random MPCD solvent,[64] which does not include hydrodynamic interactions (−HI), but it leads to similar fluid properties such as shear viscosity or mass diffusion, see Supporting Information (SI) for details. We simulated unknotted rings (denoted 0_1) and rings carrying a trefoil knot (denoted 3_1) under shear; simulations of linear polymers (denoted L) were also performed at selected parameter values, serving as tests against previously calculated quantities for this topology. To identify and locate the knotted section on the ring, we computed the Alexander polynomial for sections of the ring chosen by performing a bottom-up search, and the ends of these sections closed by minimally interfering closure,[71] returning the shortest knotted section as a result. Shear rate is normalized with each polymer's longest relaxation time τ, such that the dimensionless Weissenberg number is $Wi = \dot{\gamma}\tau$. Relevant simulation details are presented in the SI.

A (linear) polymer under shear flow is exposed to solvent-induced tension, which grows with the shear rate $\dot{\gamma}$. Knots under tension become more localized as tension grows;[39] accordingly, one expects the knot's size, expressed by the number of monomers N_k in the knotted part, to decrease monotonically with $\dot{\gamma}$ or, equivalently, with Wi. As can be seen in Figure 1, this is not the case for 3_1-rings when HI are present. Here, the knot size decreases until $Wi \cong 300$, but thereafter, the trend reverses itself and the average knot size increases again for higher values of the Weissenberg number. In the absence of HI, the knot size reaches at $Wi \cong 500$ a minimum value, $\langle N_k \rangle \cong 17$, equal to the minimum of the +HI-case and remains essentially constant at this localized configuration for higher values of the latter.

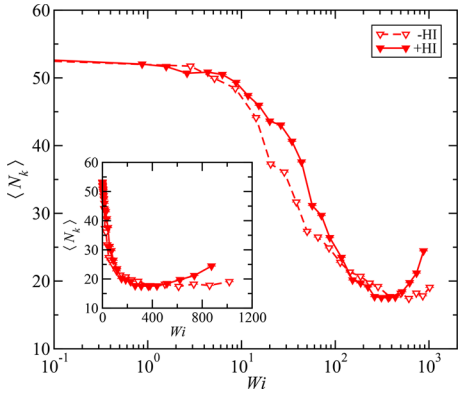

Figure 1. Averaged number of beads participating in the knot, $\langle N_k \rangle$, as a function of the Weissenberg number Wi for the 3_1-knotted ring, with and without HI. The degree of polymerization is $N = 100$. The inset shows the same curves in a linear−linear plot, to underline the extent of the nonmonotonic region for the +HI-case.

Additional insight into the statistics of knot sizes under shear is gained by considering the probability distribution of the knotted fraction, $P(N_k)$, shown in Figure 2. The distributions of

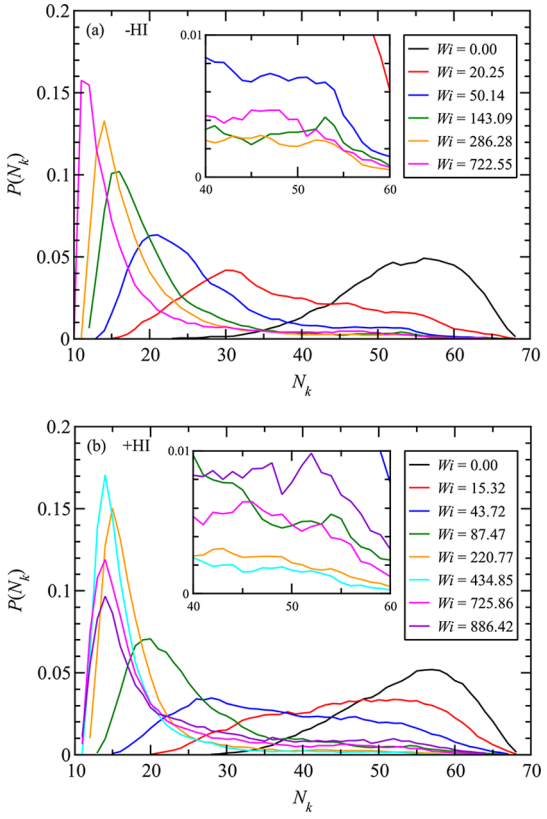

Figure 2. Probability distribution function of the knotted section size, N_k, of a 3_1-ring with $N = 100$ monomers for various values of the Weissenberg number: (a) HI excluded; (b) HI included. The insets show zooms at the regions of large knots to underline the stronger nonmonotonicity in the +HI-case.

the knot's sizes are, in general, quite broad, for any value of Wi and for both cases −HI or +HI. Significant differences between −HI and +HI arise as the Weissenberg number grows. In the −HI case, Figure 2a, the distribution of N_k is monotonically shifting toward smaller N_k values. At $Wi \cong 300$, a sharp maximum at $N_k \cong 15$ appears, which grows in height while shifting to lower N_k-values as Wi grows; excursions to configurations with $N_k \cong 60$ are still possible, see insets of Figure 2a. The +HI case, Figure 2b, is more complicated. The probability maximum moves toward lower N_k with increasing shear rate up to $Wi \approx 300$, for higher values of Wi the position of the maximum remains fixed at $N_k = 14$ and the height of the maximum decreases. This loss of weight at tight knot configurations takes place at the advantage of a gain of weight for extended knot configurations (see insets, Figure 2). However, there is no other preferred size of the knot, but all values of the knot size up to $N_k \cong 60$ get increasingly enhanced as Wi grows, pointing to the occurrence of a multitude of knot sizes, which arise from the existence of irregular dynamical patterns. We can conclude that at large shears, delocalized knot

DOI: 10.1021/acsmacrolett.8b00059
ACS Macro Lett. 2018, 7, 447−452

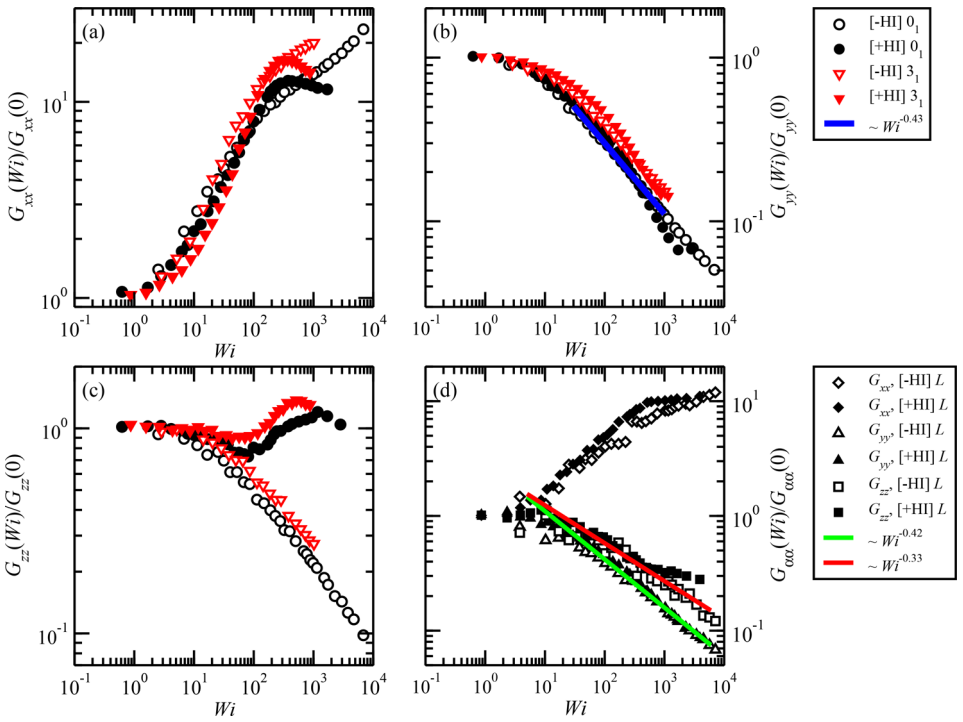

Figure 3. Normalized expectation values of the diagonal components of the gyration tensor under shear, with and without HI as functions of the Weissenberg number. (a–c) Rings 0_1 (black circles) and 3_1 (red triangles) of $N = 100$ beads in the (a) flow, (b) gradient, and (c) vorticity directions. (d) Linear polymer topology (L) of $N = 50$ monomers, for all spatial directions. Symbols are simulation results and solid lines fits to power laws.

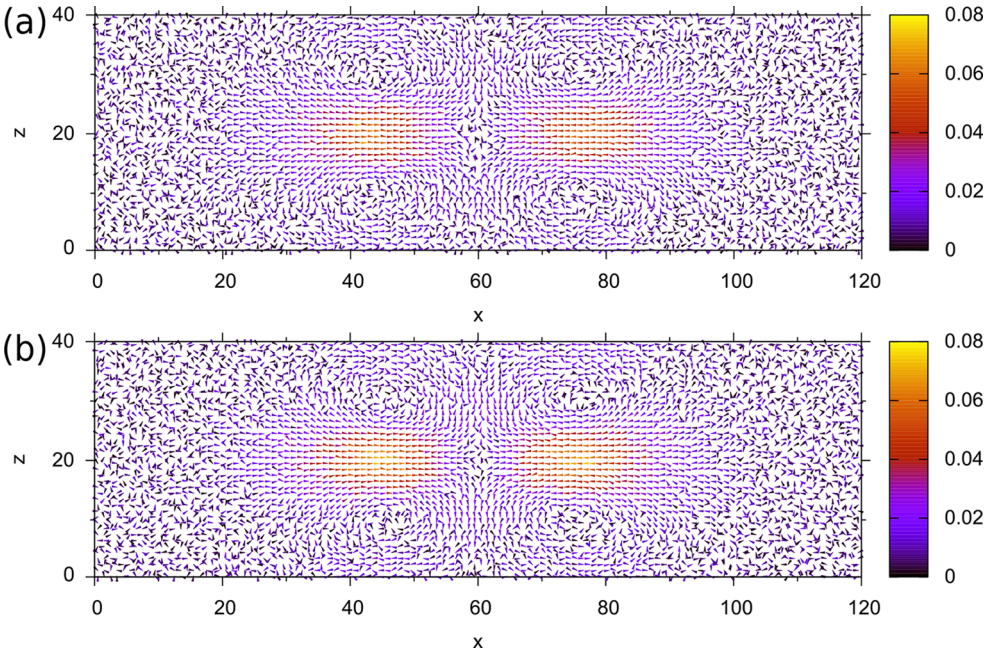

Figure 4. Solvent flow profiles on the flow (x)-vorticity (z) plane at $Wi = 500$ shearing (a) a dissolved 0_1-ring and (b) a 3_1-knotted ring. Velocity magnitudes at the color bar on the right and positions are expressed in MPCD units of a/τ_{MPCD}, where $\tau_{MPCD} = \sqrt{ma^2/k_BT}$, with $a = m = k_BT = 1$. The MPCD collision time step is $h = 0.1$.

configurations are more lasting and frequent in the presence of HI than in its absence (see SI for more details).

We focus now on the strong shear regime, $Wi > 300$. Rings display two main dynamical patterns: During the tank-treading (TT) rotation, the ring thins out, both along vorticity and gradient directions, and this shape remains approximately unchanged while all beads rotate around the vorticity axis. This type of motion becomes increasingly stable for stiffer rings.[54] A knotted ring in such TT rotation features a knot that remains strongly tight and behaves as a large bead rotating around along with all other monomers. The tumbling (TB) motion is fundamentally different. The ring adopts irregular shapes, alternating between stretched and collapsed states with a constant exchange of the beads placed in the tips of the

DOI: 10.1021/acsmacrolett.8b00059
ACS Macro Lett. 2018, 7, 447–452

elongated configurations aligned with the flow direction. The collapsed states produce an important release of tension which loosens the knots and increases their size. But most interestingly, a crucial difference appears in the presence or absence of HI. This is that while in the absence of HI both TB and TT are occurring with similar frequencies; in the presence of HI, TT motions are rare and much less stable. This property is the result of a deeper underlying mechanism: independently of the presence of knots, rings feature a nontrivial coupling between topology and hydrodynamics and the knot size of the 3_1-ring offers a clear quantitative signature of this effect.

To justify the above statements, we compute the diagonal elements of the gyration tensor $\mathcal{G}$ (defined in the SI). In Figure 3, we show a comparison of the results for rings and linear chains with and without HI. We first see that HI have no significant effect on the diagonal components of the gyration tensor for the linear (L) topology: the flow-component G_{xx} grows with Wi, whereas the gradient and vorticity components decrease, following at high Wi-values power laws that are in agreement with previous results.[72] For rings, things are very different. Although the effects of HI are small for the gradient-direction diagonal component G_{yy} shown in Figure 3b, there are dramatic differences for the vorticity direction component G_{zz}, accompanied by corresponding ones in the flow direction, G_{xx}, shown in Figure 3c and a, respectively. After a small initial shrinkage of the rings in the vorticity direction up to $Wi \cong 100$, there is a reswelling of the same, which correlates with a decrease of the extent in the flow direction, a phenomenon completely absent when HI are neglected. This is a combined effect of hydrodynamics and topology which has been already reported independently for the case of planar elongational flow, both in simulations and experiments by Hsiao et al.[59] As argued there, a ring that lies (almost) parallel to the flow-vorticity plane is experiencing a backflow of the solvent from the horseshoe-shaped regions in the flow direction back toward its interior, which escapes via the vorticity direction. It is precisely this induced flow which presses against the ring in the vorticity direction and causes a swelling, having as a secondary effect the reversal of stretching in the flow direction and the set-in of re-entrant shrinking, expressed as a maximum in the curves $G_{xx}(Wi)$ in Figure 3a.

The backflow can be explicitly calculated in our simulations by measuring the average solvent velocity field in the vorticity-flow plane, as shown in Figure 4. A strong backflow can be clearly seen in both the unknotted and the knotted cases, emerging from the two diametrically located regions around the most extended tips of the ring-shaped polymers in the flow direction. The closed polymer compresses the solvent along the x (flow)-axis, which escapes then in an expansive fashion along the z (vorticity)-axis. This escaping flow meets there the parts of the ring that lie almost parallel to the x-axis, and pushes them away along the $\pm z$-semiaxes, causing the aforementioned swelling in the vorticity direction. The absence of total flux and the system geometry, give rise to four counter-rotating vortices in diagonal positions from the box center. Further detailed results are presented in Section S4 of the SI, where the effect of varying the Weissenberg number, solvent viscosity, and box size are shown to have only a secondary, quantitative influence, which convincingly proves the existence and relevance of the backflow.

In the case of shear flow, the alignment of the ring with the flow-vorticity plane is never perfect and the oval-shaped configuration is not perfectly stable. However, the hydrodynamic mechanism plays the key role in the stage of the motion immediately after the TT-motion. During the TT-cycles, the rings resemble thin, almost planar ellipses lying on the flow-gradient plane, until spontaneous disturbances change the ring orientation, partially turning it parallel to the flow-vorticity plane. Once this happens, the topology–hydrodynamics coupling mentioned above sets in, causing the ring to swell in the vorticity direction and shrink in the flow direction. This relaxation of the ring has a number of consequences: it releases tension, thus, allowing the knot to relax toward an entropically more favored, delocalized configuration; it brings forward loose knots that remain extended for longer time intervals; and it creates swollen, more random overall ring configurations, which make the tumbling motion more chaotic, irregular, and long lasting. During this stage, the knots remain delocalized and contribute to the increase of the expectation value $\langle N_k \rangle$. Although the knots can also loosen in the absence of HI, there the TT-stages of the motion are longer, the delocalization events much more rare, and their duration shorter than in the presence of HI.

In the Supporting Information, we also provide videos showing characteristic motions of knotted and unknotted rings with and without HI. We also visualize in Section S7 one very common knot-delocalization pathway conforming to the above-mentioned scenario. The types of motion described above are common to 0_1- and 3_1-rings, and interestingly, they result in a decrease of the intrinsic viscosity and in a crossover of its dependence on Wi between two different power laws, a characteristic that again bears the unique signature of the influence of hydrodynamics. Details can be found in Section S6 of the Supporting Information. Also important to point out is that our findings are at odds with those of Chen et al.[57] who found no influence of HI on the sheared ring conformations.

To summarize, we have shown that the 3_1-knotted ring exhibits nonmonotonic behavior above Weissenberg numbers of $Wi \approx 300$ as far as size, shape, alignment, and knotted section size are concerned, and we have linked this directly to the presence of hydrodynamic interactions. With and without HI, 3_1-knotted rings under shear feature two characteristic states, one with very tight and one with delocalized knotted section, and may exhibit tank-treading or tumbling with varying probability to switch from one to the other. However, the 3_1-knotted ring's tank-treading motion is strongly suppressed in the presence of HI. A particularly relevant question arising is whether this phenomenon is generic to all types of knots. Preliminary investigations on more complex knot topologies seem to indicate that although the swelling in the vorticity direction is a common feature, the loosening of the knot also requires a braided region which is not too complex. Highly intricate knots also have tight and strongly entangled braids, whose internal friction is too strong for the knot to be relaxed by the mechanisms described above. A more detailed investigation of these questions will be the subject of further investigations, as well as additional research on possibilities to use the findings obtained in this work; for example, in the design of techniques to separate unknotted and knotted polymer rings. Other possible applications are related to the manipulation of knots under shear for rings with varying rigidity or chemical properties along their backbone.

DOI: 10.1021/acsmacrolett.8b00059
ACS Macro Lett. 2018, 7, 447–452

■ ASSOCIATED CONTENT

Supporting Information

The Supporting Information is available free of charge on the ACS Publications website at DOI: 10.1021/acsmacrolett.8b00059.

Simulation model details; knot localization procedure; supplementary plots on polymer shape, alignment and deformational resistance; effects of box size and MPCD-time step; intrinsic viscosity; TT- and TB-frequencies (PDF).

3_1-ring tumbling, knot opening, +HI: Video showing irregular motion of a 3_1-knotted ring, featuring several tumbling cycles and several events during which the knot opens up and remains in an open configuration for considerably long amounts of time. Hydrodynamic interactions are taken into account (+HI) (MPG).

3_1-ring tumbling, knot opening, +HI: Video showing a different time sequence with knot opening and tumbling events. Hydrodynamic interactions are taken into account (+HI) (MPG).

3_1-ring tumbling, −HI: Video showing a tumbling motion of a 3_1-knotted ring in the absence of hydrodynamic interactions (−HI) (MPG).

3_1-ring tank-treading, −HI: Video showing a tank-treading motion of a 3_1-knotted ring in the absence of hydrodynamic interactions (−HI) (MPG).

0_1-ring tumbling, +HI: Video showing a tumbling motion of a 0_1-ring in the presence of hydrodynamic interactions (+HI) (MPG).

0_1-ring tank-treading, +HI: Video showing a tank treading motion of a 0_1-ring in the presence of hydrodynamic interactions (+HI) (MPG).

0_1-ring tumbling, −HI: Video showing a tumbling motion of a 0_1-ring in the absence of hydrodynamic interactions (−HI) (MPG).

0_1-ring tank-treading, −HI: Video showing a tank-treading motion of a 0_1-ring in the absence of hydrodynamic interactions (−HI) (MPG).

■ AUTHOR INFORMATION

Corresponding Author

*E-mail: maximilian.liebetreu@univie.ac.at.

ORCID

Maximilian Liebetreu: 0000-0001-8374-8476

Christos N. Likos: 0000-0003-3550-4834

Notes

The authors declare no competing financial interest.

■ ACKNOWLEDGMENTS

We thank Luca Tubiana for providing and explaining his LocKnot program for efficient recognition and localization of knotted sections on polymer structures, as well as Dimitris Vlassopoulos for a critical reading of the manuscript and helpful comments. The computational results presented have been achieved in part using the Vienna Scientific Cluster (VSC). M.L. has been supported in part by the uni:docs Doctoral Fellowship Programme of the University of Vienna. EU-COST action MP1305 "Flowing Matter" is kindly acknowledged.

■ REFERENCES

(1) Winkler, R. G.; Fedosov, D. A.; Gompper, G. Dynamical and rheological properties of soft colloid suspensions. *Curr. Opin. Colloid Interface Sci.* **2014**, *19*, 594−610.

(2) Vlassopoulos, D.; Cloitre, M. Tunable rheology of dense soft deformable colloids. *Curr. Opin. Colloid Interface Sci.* **2014**, *19*, 561−574.

(3) Vologodskii, A. V.; Lukashin, A. V.; Frank-Kamenetskii, M. D.; Anshelevich, V. V. The knot problem in statistical mechanics of polymer chains. *Sov. Phys. JETP* **1974**, *39*, 1059−1063.

(4) Frank-Kamenetskii, M. D.; Lukashin, A. V.; Vologodskii, A. V. Statistical mechanics and topology of polymer chains. *Nature* **1975**, *258*, 398−402.

(5) Katritch, V.; Bednar, J.; Michoud, D.; Scharein, R. G.; Dubochet, J.; Stasiak, A. Geometry and physics of knots. *Nature* **1996**, *384*, 142−145.

(6) Micheletti, C.; Marenduzzo, D.; Orlandini, E. Polymers with spatial or topological constraints: Theoretical and computational results. *Phys. Rep.* **2011**, *504*, 1−73.

(7) Koniaris, K.; Muthukumar, M. Knottedness in ring polymers. *Phys. Rev. Lett.* **1991**, *66*, 2211−2214.

(8) Wasserman, S. A.; Cozzarelli, N. R. Biochemical Topology: Applications to DNA Recombination and Replication. *Science* **1986**, *232*, 951−960.

(9) Rybenkov, V. V.; Cozzarelli, N. R.; Vologodskii, A. V. Probability of DNA knotting and the effective diameter of the DNA double helix. *Proc. Natl. Acad. Sci. U. S. A.* **1993**, *90*, 5307−5311.

(10) Micheletti, C.; Marenduzzo, D.; Orlandini, E.; Sumners, D. W. Simulations of Knotting in Confined Circular DNA. *Biophys. J.* **2008**, *95*, 3591−3599.

(11) Virnau, P.; Mirny, L. A.; Kardar, M. Intricate Knots in Proteins: Function and Evolution. *PLoS Comput. Biol.* **2006**, *2*, e122.

(12) Sułkowska, J. I.; Noel, J. K.; Onuchic, J. N. Energy landscape of knotted proetin folding. *Proc. Natl. Acad. Sci. U. S. A.* **2012**, *109*, 17783−17788.

(13) Dabrowski-Tumanski, P.; Sułkowska, J. I. Topological knots and links in proteins. *Proc. Natl. Acad. Sci. U. S. A.* **2017**, *114*, 3415−3420.

(14) Arai, Y.; Yashuda, R.; Akashi, K.; Harada, Y.; Miyata, H.; Kinoshita, K., Jr.; Itoh, H. Tying a molecular knot with optical tweezers. *Nature* **1999**, *399*, 446−448.

(15) Bao, X. R.; Lee, H. J.; Quake, S. R. Behavior of Complex Knots in Single DNA Molecules. *Phys. Rev. Lett.* **2003**, *91*, 265506.

(16) Leigh, D.; Woltering, S. L.; Fielden, S. Molecular Knots. *Angew. Chem., Int. Ed.* **2017**, *56*, 11166−11194.

(17) Grosberg, A. Y.; Feigel, A.; Rabin, Y. Flory-type theory of a knotted ring polymer. *Phys. Rev. E: Stat. Phys., Plasmas, Fluids, Relat. Interdiscip. Top.* **1996**, *54*, 6618−6622.

(18) Grosberg, A. Y. Critical Exponents for Random Knots. *Phys. Rev. Lett.* **2000**, *85*, 3858−3861.

(19) Katritch, V.; Olson, W. K.; Vologodskii, A.; Dubochet, J.; Stasiak, A. Tightness of random knotting. *Phys. Rev. E: Stat. Phys., Plasmas, Fluids, Relat. Interdiscip. Top.* **2000**, *61*, 5545−5549.

(20) Grosberg, A. Y.; Rabin, Y. Metastable tight knots in a wormlike polymer. *Phys. Rev. Lett.* **2007**, *99*, 217801.

(21) Mansfield, M. L.; Douglas, J. F. Properties of knotted ring polymers. I. Equilibrium dimensions. *J. Chem. Phys.* **2010**, *133*, 044903.

(22) Mansfield, M. L.; Douglas, J. F. Properties of knotted ring polymers. II. Transport properties. *J. Chem. Phys.* **2010**, *133*, 044904.

(23) Tubiana, L.; Rosa, A.; Fragiacomo, F.; Micheletti, C. Spontaneous knotting and unknotting of flexible linear polymers: equilibrium and kinetic aspects. *Macromolecules* **2013**, *46*, 3669−3678.

(24) Narros, A.; Moreno, A. J.; Likos, C. N. Effects of Knots on Ring Polymers in Solvents of Varying Quality. *Macromolecules* **2013**, *46*, 3654−3668.

(25) Dai, L.; Doyle, P. S. Effects of intrachain interactions on the knot size of a polymer. *Macromolecules* **2016**, *49*, 7581−7587.

(26) Quake, S. R. Topological Effects of Knots in Polymers. *Phys. Rev. Lett.* **1994**, *73*, 3317−3320.

DOI: 10.1021/acsmacrolett.8b00059
ACS Macro Lett. 2018, 7, 447−452

(27) Lai, P.-Y. Dynamics of polymer knots at equilibrium. *Phys. Rev. E: Stat. Phys., Plasmas, Fluids, Relat. Interdiscip. Top.* **2002**, *66*, 021805.
(28) Sheng, Y.-J.; Cheng, K.-L. Polymer knot confined in a tube: Statics and relaxation dynamics. *Phys. Rev. E: Stat. Phys., Plasmas, Fluids, Relat. Interdiscip. Top.* **2001**, *65*, 011801.
(29) Micheletti, C.; Orlandini, E. Numerical study of linear and circular model DNA chains confined in a slit: metric and topological properties. *Macromolecules* **2012**, *45*, 2113−2121.
(30) Dai, L.; van der Maarel, J.; Doyle, P. S. Effect of nanoslit confinement on the knotting probability of circular DNA. *ACS Macro Lett.* **2012**, *1*, 732−736.
(31) Nakajima, C. H.; Sakaue, T. Localization and size distribution of a polymer knot confined in a channel. *Soft Matter* **2013**, *9*, 3140−3146.
(32) D' Adamo, G.; Micheletti, C. Molecular Crowding Increases Knots Abundance in Linear Polymers. *Macromolecules* **2015**, *48*, 6337−6346.
(33) Dai, L.; Renner, C. B.; Doyle, P. S. Metastable knots in confined semiflexible chains. *Macromolecules* **2015**, *48*, 2812−2818.
(34) Klotz, A. R.; Narsimhan, V.; Soh, B. W.; Doyle, P. S. Dynamics of DNA Knots During Chain Relaxation. *Macromolecules* **2017**, *50*, 4074−4082.
(35) Marenda, M.; Orlandini, E.; Micheletti, C. Sorting ring polymers by knot type with modulated nanochannels. *Soft Matter* **2017**, *13*, 795−802.
(36) Saitta, A. M.; Soper, P. D.; Wasserman, E.; Klein, M. L. Influence of a knot on the strength of a polymer strand. *Nature* **1999**, *399*, 46−48.
(37) Sheng, Y.-J.; Lai, P.-Y.; Tsao, H.-K. Deformation of a stretched polymer knot. *Phys. Rev. E: Stat. Phys., Plasmas, Fluids, Relat. Interdiscip. Top.* **2000**, *61*, 2895−2901.
(38) Farago, O.; Kantor, Y.; Kardar, M. Pulling knotted polymers. *EPL* **2002**, *60*, 53−59.
(39) Matthews, R.; Louis, A. A.; Likos, C. N. Effect of bending rigidity on the knotting of a polymer under tension. *ACS Macro Lett.* **2012**, *1*, 1352−1356.
(40) Poier, P.; Likos, C. N.; Matthews, R. Influence of Rigidity and Knot Complexity on the Knotting of Confined Polymers. *Macromolecules* **2014**, *47*, 3394−3400.
(41) Caraglio, M.; Micheletti, C.; Orlandini, E. Stretching Response of Knotted and Unknotted Polymer Chains. *Phys. Rev. Lett.* **2015**, *115*, 188301.
(42) Matthews, R.; Louis, A. A.; Yeomans, J. M. Knot-Controlled Ejection of a Polymer from a Virus Capsid. *Phys. Rev. Lett.* **2009**, *102*, 088101.
(43) Rosa, A.; Di Ventra, M.; Micheletti, C. Topological Jamming of Spontaneously Knotted Polyelectrolyte Chains Driven Through a Nanopore. *Phys. Rev. Lett.* **2012**, *109*, 118301.
(44) Marenduzzo, D.; Micheletti, C.; Orlandini, E.; Sumners, D. W. Topological friction strongly affects viral DNA ejection. *Proc. Natl. Acad. Sci. U. S. A.* **2013**, *110*, 20081−20086.
(45) Trefz, B.; Siebert, J.; Virnau, P. How molecular knots can pass through each other. *Proc. Natl. Acad. Sci. U. S. A.* **2014**, *111*, 7948−7951.
(46) Suma, A.; Rosa, A.; Micheletti, C. Pore Translocation of Knotted Polymer Chains: How Friction Depends on Knot Complexity. *ACS Macro Lett.* **2015**, *4*, 1420−1424.
(47) Narsimhan, V.; Renner, C. B.; Doyle, P. S. Translocation dynamics of knotted polymers under a constant or periodic external field. *Soft Matter* **2016**, *12*, 5041−5049.
(48) Plesa, C.; Verschueren, D.; Pud, S.; van der Torre, J.; Ruitenberg, J. W.; Witteveen, M. J.; Jonsson, M. P.; Grosberg, A. Y.; Rabin, Y.; Dekker, C. Direct observation of DNA knots using a solid-state nanopore. *Nat. Nanotechnol.* **2016**, *11*, 1093−1098.
(49) Suma, A.; Micheletti, C. Pore translocation of knotted DNA rings. *Proc. Natl. Acad. Sci. U. S. A.* **2017**, *114*, E2991−E2997.
(50) Kivotides, D.; Wilkin, S. L.; Theofanous, T. G. Entangled chain dynamics of polymer knots in extensional flow. *Phys. Rev. E* **2009**, *80*, 041808.
(51) Renner, C. B.; Doyle, P. S. Untying Knotted DNA with Elongational Flows. *ACS Macro Lett.* **2014**, *3*, 963−967.
(52) Matthews, R.; Louis, A. A.; Yeomans, J. M. Complex dynamics of knotted filaments in shear flow. *EPL* **2010**, *92*, 34003.
(53) Kuei, S.; Słowicka, A. M.; Ekiel-Jeżewska, M. L.; Wajnryb, E.; Stone, H. A. Dynamics and topology of a flexible chain: knots in steady shear flow. *New J. Phys.* **2015**, *17*, 053009.
(54) Lang, P. S.; Obermayer, B.; Frey, E. Dynamics of a semiflexible polymer or polymer ring in shear flow. *Phys. Rev. E* **2014**, *89*, 022606.
(55) Chen, W.; Chen, J.; An, L. Tumbling and tank-treading dynamics of individual ring polymers in shear flow. *Soft Matter* **2013**, *9*, 4312−4318.
(56) Chen, W.; Li, Y.; Zhao, H.; Liu, L.; Chen, J.; An, L. Conformations and dynamics of single flexible ring polymers in simple shear flow. *Polymer* **2015**, *64*, 93−99.
(57) Chen, W.; Zhao, H.; Liu, L.; Chen, J.; Li, Y.; An, L. Effects of excluded volume and hydrodynamic interaction on the deformation, orientation and motion of ring polymers in shear flow. *Soft Matter* **2015**, *11*, 5265−5273.
(58) Li, Y.; Hsiao, K.-W.; Brockman, C. A.; Yates, D. Y.; Robertson-Anderson, R.; Kornfield, J. A.; San Francisco, M. J.; Schroeder, C. M.; McKenna, G. B. When Ends Meet: Circular DNA Stretches Differently in Elongational Flows. *Macromolecules* **2015**, *48*, 5997−6001.
(59) Hsiao, K.-W.; Schroeder, C. M.; Sing, C. E. Ring Polymer Dynamics are Governed by a Coupling between Architecture and Hydrodynamic Interactions. *Macromolecules* **2016**, *49*, 1961−1971.
(60) Malevanets, A.; Kapral, R. Mesoscopic model for solvent dynamics. *J. Chem. Phys.* **1999**, *110*, 8605−8613.
(61) Gompper, G.; Ihle, T.; Kroll, D.; Winkler, R. Multi-Particle Collision Dynamics - a Particle-Based Mesoscale Simulation Approach to the Hydrodynamics of Complex Fluids. *Adv. Polym. Sci.* **2008**, *221*, 1−91.
(62) Mussawisade, K.; Ripoll, M.; Winkler, R. G.; Gompper, G. Dynamics of polymers in a particle-based mesoscopic solvent. *J. Chem. Phys.* **2005**, *123*, 144905.
(63) Ripoll, M.; Winkler, R. G.; Gompper, G. Star Polymers in Shear Flow. *Phys. Rev. Lett.* **2006**, *96*, 188302.
(64) Ripoll, M.; Winkler, R. G.; Gompper, G. Hydrodynamic screening of star polymers in shear flow. *Eur. Phys. J. E: Soft Matter Biol. Phys.* **2007**, *23*, 349−354.
(65) Lees, A. W.; Edwards, S. F. The computer study of transport processes under extreme conditions. *J. Phys. C: Solid State Phys.* **1972**, *5*, 1921−1929.
(66) Huang, C. C.; Chatterji, A.; Sutmann, G.; Gompper, G.; Winkler, R. Cell-level canonical sampling by velocity scaling for multiparticle collision dynamics simulations. *J. Comput. Phys.* **2010**, *229*, 168−177.
(67) Kremer, K.; Grest, G. S. Dynamics of entangled linear polymer melts: A molecular-dynamics simulation. *J. Chem. Phys.* **1990**, *92*, 5057−5086.
(68) Poier, P.; Likos, C. N.; Moreno, A. J.; Blaak, R. An Anisotropic Effective Model for the Simulation of Semiflexible Ring Polymers. *Macromolecules* **2015**, *48*, 4983−4997.
(69) Verlet, L. Computer Experiments on Classical Fluids. I. Thermodynamical Properties of Lennard-Jones Molecules. *Phys. Rev.* **1967**, *159*, 98−103.
(70) Grotendorst, J.; Sutmann, G.; Gompper, G.; Marx, D. *Hierarchical Methods for Dynamics in Complex Molecular Systems Lecture Notes*; IAS Series; Forschungszentrum Jülich: Jülich, 2012; Vol. *10*; pp 417−444.
(71) Tubiana, L.; Orlandini, E.; Micheletti, C. Probing the Entanglement and Locating Knots in Ring Polymers: A Comparative Study of Different Arc Closure Schemes. *Prog. Theor. Phys. Suppl.* **2011**, *191*, 192−204.
(72) Huang, C.-C.; Winkler, R. G.; Sutmann, G.; Gompper, G. Semidilute Polymer Solutions at Equilibrium and under Shear Flow. *Macromolecules* **2010**, *43*, 10107−10116.

DOI: 10.1021/acsmacrolett.8b00059
ACS Macro Lett. 2018, 7, 447−452